Peertechz

Journal of Biology and Medicine
submitpaper@peertechz.com
MEDICAL GROUP
JOURNAL OF Biology and Medicine OPEN ACCESS JOURNAL
ISSN: 2688-8408 DOI: https://dx.doi.org/10.17352/jbm

Research Article

Synthesis, characterization, anti-cancer evaluation, and DNA-binding study of new bay-substituted perylene derivatives

Arwa Abourajab[1], S Melika Mostafanejad[1], Meltem Dinleyici[1], Basma Al-Khateeb[1], Imge Kunter[2], Sukru Tuzmen[3] and Huriye Icil[1]*

[1]Department of Chemistry, Faculty of Arts and Science, Eastern Mediterranean University, 99628, Famagusta N Cyprus, Mersin 10, Turkey
[2]Faculty of Pharmacy, Eastern Mediterranean University, 99628, Famagusta N Cyprus, Mersin 10, Turkey
[3]Faculty of Dentistry, Eastern Mediterranean University, 99628, Famagusta N Cyprus, Mersin 10, Turkey

Received: 12 July, 2023
Accepted: 20 July, 2023
Published: 21 July, 2023

***Corresponding authors:** Dr. Huriye Icil, Professor, Department of Chemistry, Faculty of Arts and Science, Eastern Mediterranean University, 99628, Famagusta N Cyprus, Mersin 10, Turkey, Tel: 00903926301085; E-mail: huriye.icil@emu.edu.tr

ORCiD: https://orcid.org/0000-0002-3389-6734

Keywords: Perylene bisanhydride; Guanine; PCR; Oligonucleotide; Electrophoresis; MTT assay

Abstract

Two new perylene derivatives 1,7-di(3,5-diamino-pyrimidoxyl) perylene-3,4,9,10- tetracarboxylic acid bisanhydride (**4**) and 1,7-di(2-[3-[(4-amino-2-methylpyrimidin-5-yl)methyl]-4-methyl-1,3-thiazol-3-ium-5-yl]) ethoxyperylene-3,4,9,10-tetracarboxylic bisanhydride (**6**) have been synthesized. We aimed to study their interactions with G-quadruplex (G4) structures as potent G4 ligands and telomerase inhibitors. We used a PCR-amplified guanine-rich region from the human beta-globin gene, oligonucleotide from human telomeres (a-coreTT), an oncogene (c-kit), and SK-HEP-1 adenocarcinoma cells to characterize those compounds' binding and stabilizing abilities to G4 structures and anti-cancer potential. All results obtained through UV-visible and fluorescence spectroscopies, agarose gel electrophoresis, and MTT assay on SK-HEP-1 adenocarcinoma cells were in good agreement. Compounds **4** and **6** are promising DNA-binding and cytotoxic compounds with a relatively antiproliferative effect on the selected tumour. In all studies, the formal positive charge carrier, compound **6**, showed higher activity in terms of anti-cancer effects. These results may help elucidate the feasibility of the perylene derivatives as future chemo-therapeutic agents.

Introduction

Perylene derivatives are intensively studied as transcriptional regulators and telomerase inhibitors [1-5]. The guanine-rich regions of the human genome are the critical point in forming four-stranded G4 structures [6,7]. Guanine bases are the focal point because they create a type of bonding called Hoogsteen hydrogen bonding, enabling them to form secondary structures different from the Watson-Crick DNA double helix [8,9]. Each guanine base forms two Hoogsteen hydrogen bonds with two adjacent guanine bases. Notably, four guanines associate through eight Hoogsteen hydrogen bonds, resulting in a planar ring structure called a guanine tetrad [10]. The resulting strong van der Waals attractions cause the tetramers to get stacked on top of each other and form a G4 structure [6]. The small molecules facilitating and stabilizing G4 structures are studied intensively. G4 structures do not distribute randomly throughout the human genome; their formation could occur in the nucleus during transcription and replication or outside the nucleus during translation [11]. The TTAGGG tandem repeat sequence in human telomeres is rich in repetitive guanine bases [12], and G4 structures were reported

Citation: Abourajab A, Mostafanejad SM, Dinleyici M, Al-Khateeb B, Kunter I, et al. (2023) Synthesis, characterization, anti-cancer evaluation, and DNA-binding study of new bay-substituted perylene derivatives. J Biol Med 7(1): 031-043. DOI: https://dx.doi.org/10.17352/jbm.000039

throughout the human telomeres [13]. Oncogenes such as c-kit with guanine-rich promoter regions have been investigated and published [14-16].

Several classes of organic molecules were studied for their G4 binding selectivity [17-21]. Common characteristics of the organic molecules studied for this purpose include a large aromatic core with delocalized π-electrons for the stacking interactions with the guanine tetrads [22]. Further, the side chains with a preferably positive charge for interacting with the negatively charged DNA grooves [23] and good water solubility are essential for investigation in cell lines [24].

Several research groups reported perylene derivatives as G4 ligands and telomerase inhibitors [25-27]. Notably, the aromatic core of perylene binds to the outer G-tetrad of the G4 through π-π interactions and the hydrophilic side chains interact with the DNA grooves. Perylene derivatives are advantageous for interaction studies because of different properties, such as the modifications done to obtain symmetrical/asymmetrical [28] or cyclic [29] analogues or alterations done by adding charged/uncharged, long/short, weakly/strongly essential [23] substituents or even enlarging their cores [30].

Extending the aromatic core or increasing the polar side chains on the organic structures enhances G4 selectivity [31]. The cytotoxicity of several perylene derivatives was evaluated in various cancer cell lines [32]. A prototypical perylene diimide (PIPER) was used to suppress telomerase and induce telomere shortening in lung and prostate cancer cells [2].

Herein, the design and synthesis of two bay-substituted perylene bisanhydrides: 1,7-di(3,5-diamino-pyrimidoxyl) perylene-3,4,9,10- tetracarboxylic acid bisanhydride (**4**) and 1,7-di(2-[3-[(4-amino-2-methylpyrimidin-5-yl)methyl]-4-methyl-1,3-thiazol-3-ium-5-yl]) ethoxyperylene-3,4,9,10-tetracarboxylic bisanhydride (**6**) was reported (Scheme **1**). Interactions with G4 structures as G4 ligands were studied. The substituents at the bay position were specifically selected. The two perylene derivatives have the same aromatic core but different side chains at the bay positions. Notably, both compounds have the potential to form hydrogen bonds and π-π intermolecular interactions (N-H....O, and N-H....N) (Schemes 1, 2. S1 and S2) [33]. Additionally, compound **6** has a positive charge on its bay substituent. Finally, the compounds` solubility in the Tris-HCl buffer solution was sufficient for the experimental studies. A PCR-amplified guanine-rich region from the human beta-globin gene, an oligonucleotide from human telomeres, and an oncogene was used to study those compounds' binding and stabilizing abilities to G4 structures. Investigations were performed via UV-visible and fluorescence spectroscopies, agarose gel electrophoresis, and MTT assay on SK-HEP-1 adenocarcinoma cells. The oligonucleotides (5`-3`) PCO3 (F) (ACACAACTGTGTTCACTAGC), CD6 (R) (ATTCGTCTGTTTCCCATTCTAAAC), a-coreTT (AGGGTTAGGGTTAGGGTTAGGGTT) and c-kit (AGGGAGGGCGCTGGGAGGAGGAGGG) were used in our investigations. The human hepatic adenocarcinoma cell line, SK-HEP-1 was used in the MTT assay. All the experimental and theoretical results and their consistency are discussed in detail.

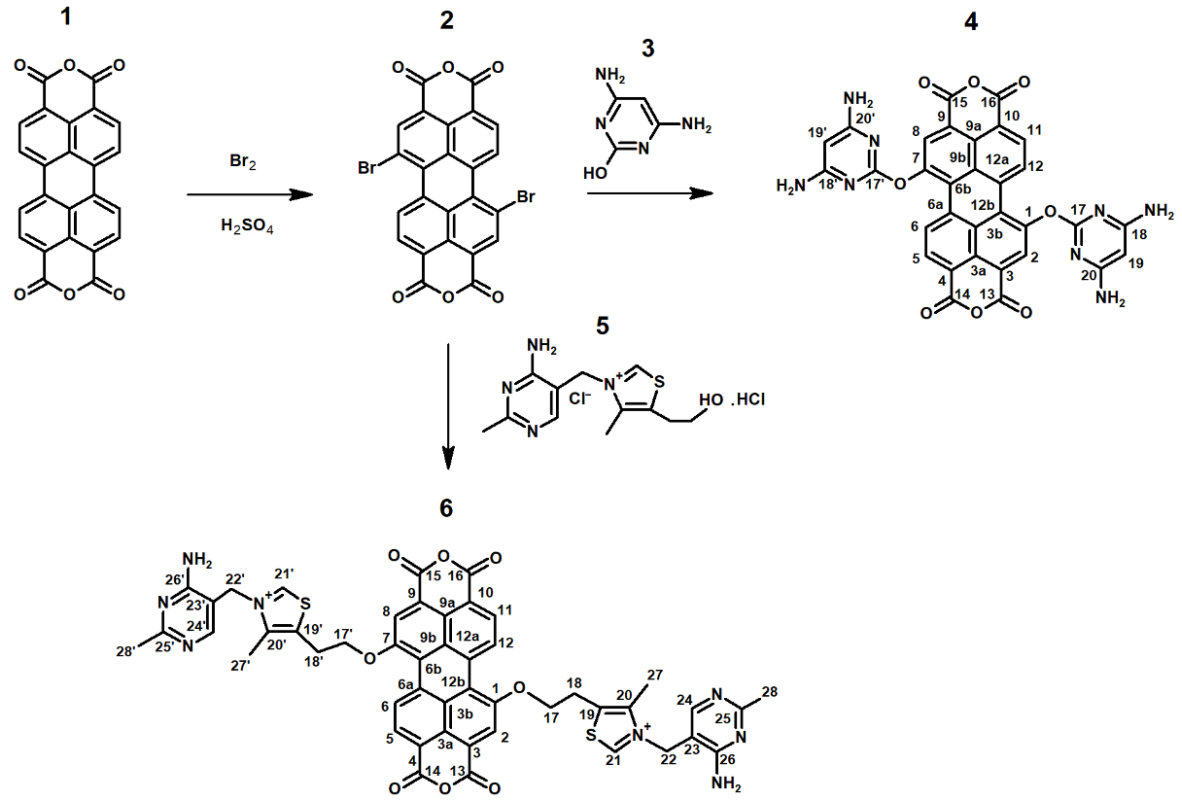

Scheme 1: The synthetic routes for the preparation of compounds **4** and **6**.

Citation: Abourajab A, Mostafanejad SM, Dinleyici M, Al-Khateeb B, Kunter I, et al. (2023) Synthesis, characterization, anti-cancer evaluation, and DNA-binding study of new bay-substituted perylene derivatives. J Biol Med 7(1): 031-043. DOI: https://dx.doi.org/10.17352/jbm.000039

Materials and methods

Materials and equipment

The DNA oligonucleotides were purchased from Oligomer Biotechnology (Çankaya, Ankara) and used without further purification. The Blirt 50X Tris-acetate-EDTA (TAE) buffer, Blirt 2xPCR TaqNova-Red- Master mix with Taq polymerase (RP85T), Blirt 2'-deoxynucleoside 5'-triphosphates (dNTPs) mix and Blirt Extractme DNA clean-up & gel-out kit were purchased from En-Ergon Scientific (Nicosia, Cyprus). Biorad 5x Orange G Loading Dye, Biorad Genes in a Bottle Lysis Buffer, Axygen 100 bp DNA ladder, Invitrogen UltraPure™ Agarose, and Thermo Scientific Proteinase K were used.

^{1}H NMR spectra were recorded on Bruker spectrometer (^{1}H, 500 MHz) in the solvent mixture $CDCl_3$ and CF_3COOD (3:1) using TMS as an internal standard. Elemental analyses were measured on a Carlo Erba-1106 (C, H, and N) elemental analyzer. FT-IR spectroscopic measurements were carried out at ambient conditions as KBr pellets using a JASCO FT-IR-6200 spectrophotometer. UV-vis spectroscopy was performed using Varian Cary-100 Spectrophotometer, and fluorescence emission data were collected using a Varian Cary Eclipse Spectrophotometer. The differential scanning calorimetry (DSC) and thermogravimetric analysis (TGA) thermograms were obtained from Perkin Elmer/DSC/Jade DSC under nitrogen and Perkin Elmer/TGA/Pyris 1 under an oxygen atmosphere, respectively, with a heating rate of 10 °C min^{-1}. The agarose gel was visualized with Gel Documentation & Analysis System (Beijing Liuyi Instrument Factory).

Synthesis

Synthesis of 1,7-di(3,5-diamino-pyrimidoxyl)perylene-3,4,9,10- tetracarboxylic acid bisanhydride (4): 1,7-Dibromoperylene-3,4,9,10-tetracarboxylic acid bisanhydride (**2**, 1.00 g, 1.82 mmol), 2,4-diamino-6-hydroxypyrimidine (**3**, 0.80 g, 5.45 mmol), and K_2CO_3 (0.62 g, 4.50 mmol) were stirred under argon atmosphere and at room temperature in 80 mL DMF for a 1 h period. The reaction mixture was then heated to reflux and continued for 10 h. After cooling to room temperature, the solution was poured into a mixture of cold acetic acid/cold water (100 mL, 1:1 by volume). The precipitate was filtered off, thoroughly washed with several portions of hot water, and dried in a vacuum oven to give the crude product. Finally, the dark purple crude product was purified by repeated recrystallization from N, N-dimethylacetamide to obtain pure product **4** as a black powder (0.78 g, 1.20 mmol, 65 %).

FT-IR (Figure 1a KBr, thin film, cm^{-1}): ν = 3385 (N – H stretch), 3015 (aromatic C-H stretch), 1756 and 1706 (anhydride C = O stretch), 1630 (C = N stretch), 1587 (aromatic C = C stretch), 1392 and 1314 (amine C–N stretch), 1249 (ether C–O–C stretch), 1010 (anhydride C–O–C stretch), 766 (aromatic C–H bend). UV-Vis (Figure 2a, NMP): λ_{max} (nm) (ε) = 306, 468, 518 (9500), 664, 746. Fluorescence (Figure 2b, NMP, λ_{exc} = 485 nm): λ_{max} (nm) = 566. Fluorescence quantum yield (Table **1**, c = 1 × 10^{-6} M in TCE, reference N,N′-bis-dodecyl-3,4,9,10-perylenebis(dicarboximide) with Φ_f = 100 %, $\lambda_{exc.}$ = 485 nm) = 15 %. MS (MALDI-TOF, Figure **S1**): m/z = 638.43 [M-2]. Anal. Calcd. for $C_{32}H_{16}N_8O_8$, (M_w, 640.50): C, 59.63; H,3.13; N 17.38. Found: C, 59.51; H, 3.04; N, 17.42.

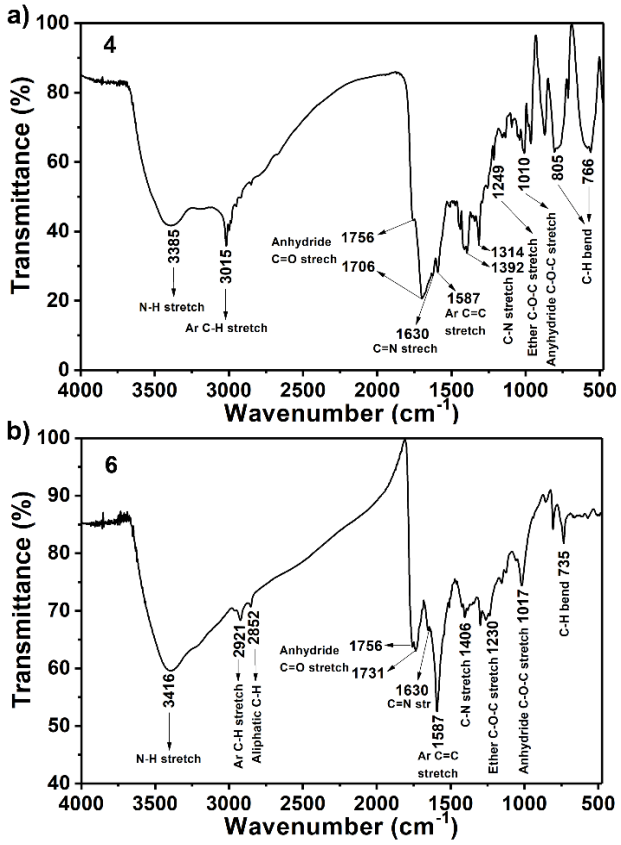

Figure 1: FTIR spectra of compound **4** (a) and **6** (b).

Synthesis of 1,7-di(2-[3-[(4-amino-2-methylpyrimidin-5-yl)methyl]-4-methyl-1,3-thiazol-3-ium-5-yl]) ethoxyperylene-3,4,9,10-tetracarboxylic bisanhydride (6): 1,7-Dibromoperylene-3,4,9,10-tetracarboxylic acid bisanhydride (**2**, 1.00 g, 1.82 mmol), thiamine chloride hydrochloride (**5**, 1.80 g, 5.40 mmol), and K_2CO_3 (0.63 g, 4.60 mmol) were stirred under argon atmosphere and at room temperature in 80 mL DMF for a 2 h period. The reaction mixture was then heated to reflux and continued for 15 h. After cooling to room temperature, the solution was poured into cold, acetic acid/cold water (100 mL, 1:1 by volume). After the completion of the reaction, the mixture was allowed to cool down to -8 °C overnight. The precipitate was filtered off, washed with several portions of hot water, and dried in a vacuum oven to give the crude product. Finally, the dark purple crude product was purified by repeated recrystallization from N, N-dimethylacetamide to obtain pure product **6** as a black powder (1.21 g, 1.32 mmol, 64 %).

^{1}H NMR (400 MHz, $CDCl_3$:CF_3COOD (3:1)): δ_H (ppm) = 9.30 (s, 2H, H-C(2), H-C(8)), 8.86 (d, 4H, H-C(5), H-C(6), H-C(11), H-C(12)), 8.84 (s, 4H, NH_2 (C26), NH_2 (C26`)), 7.19 (s, 2H, H-C(24), H-C(24`)), 3.71 (s, 4H, H-C(22), H-C(22`)), 3.25 (s, 6H, H-C(28), H-C(28`), 3.00 (s, 6H, H-C(27), H-C(27`), 2.71 (t, 2H, H-C(17), H-C(17`)) 2.70 (t, 2H, H-C(18), H-C(18`)).

Citation: Abourajab A, Mostafanejad SM, Dinleyici M, Al-Khateeb B, Kunter I, et al. (2023) Synthesis, characterization, anti-cancer evaluation, and DNA-binding study of new bay-substituted perylene derivatives. J Biol Med 7(1): 031-043. DOI: https://dx.doi.org/10.17352/jbm.000039

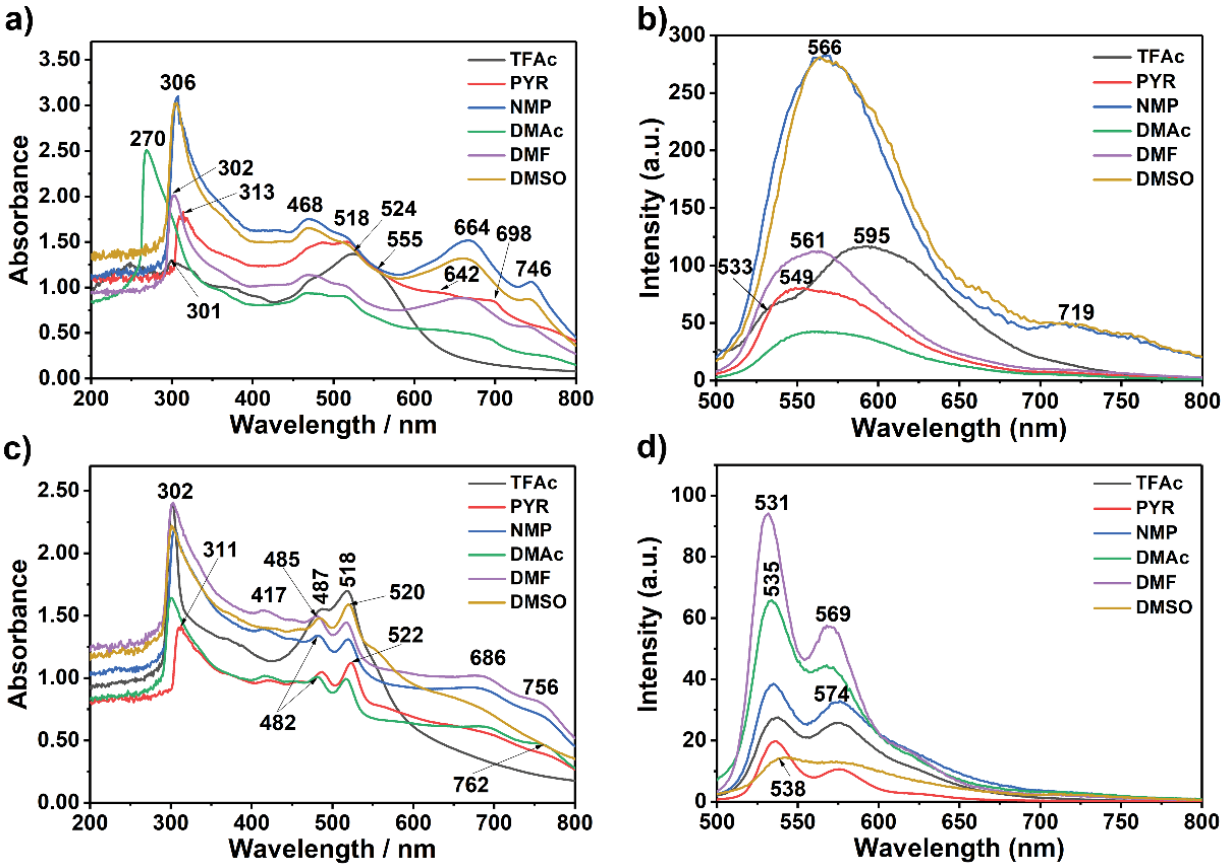

Figure 2: Absorption (a and c) and emission (b and d) spectra (λ_{exc} = 485 nm) of **4** and **6** in various solvents.

FTIR (Figure 1b, KBr, thin film, cm^{-1}): 3416 (N–H stretch), 2921 (aromatic C–H stretch), 2852 (aliphatic C–H stretch), 1756 and 1731 (anhydride C=O stretch), 1587 (aromatic C=C stretch), 1406 (C–N stretch), 1230 (ether C–O–C stretch), 1017 (anhydride C - O - C stretch), 735 (aromatic C - H bend). UV–vis (Figure 2c, NMP) λ_{max}, (nm): 302, 417, 487, 518 (12000), 686, 756. Fluorescence (Figure 2d, NMP) λ_{max}, (nm): 531, 574. Fluorescence quantum yield (Table 1, c = 1 × 10^{-6} M in TCE, reference N,N′-bis-dodecyl-3,4,9,10-perylenebis(dicarboximide) with Φ_f = 100 %, $\lambda_{exc.}$ = 485 nm) = 20 %. Anal. Calcd. For $C_{48}H_{38}Cl_2N_8O_8S_2$, ($M_w$, 989.90): C, 58.24; H, 3.87; N 11.32. Found: C, 58.31; H, 3.64; N, 11.40.

Table 1: Qualitative solubility (solubility/color)[a] of 4 and 6 in various solvents.

Solvent	4	6
TFAc[b]	(+) purple	(+) wine red
m-Cresol	(+) dark red	(− +) purple brown
PYR[c]	(+) dark brown	(+) dark brown
NMP[d]	(+) dark brown	(+) dark brown
Methanol	(− +) pale brown	(−)
DMAC[e]	(+) dark brown	(+) dark brown
DMF[f]	(+) dark brown	(+) dark brown
DMSO[g]	(+) dark brown	(+) dark brown

Note: [a]A measured concentration of 1 mg mL^{-1} in solvents at 25 ℃. (+ +): soluble at room temperature. (–+): partially soluble on heating at 35 ℃ in sonicator; (+ –): mostly soluble on heating at 35 ℃ in sonicator; (–): insoluble. [b]TFAc: Trifluoroacetate. [c]PYR: Pyridine. [d]NMP: N-methylpyrrolidinone. [e]DMF: N,N-dimethylformamide. [f]DMAC: N,N-dimethylacetamide. [g]DMSO: Dimethyl sulfoxide.

DNA extraction

The DNA extraction protocol was carried out with permission from the Eastern Mediterranean University Research and Publication Ethics Board. The DNA extraction protocol was carried out according to the manufacturer's protocol (EDVO-Kit #119 Genes in a TubeTM).

Polymerase Chain Reaction (PCR)

Polymerase Chain Reaction (PCR) [34] was carried out for a guanine-rich region of the beta-globin gene (exon I, exon II, and 60 bp of intron II after exon II) from the isolated human DNA. PCR amplification was performed with 1X PCR buffer, 5 u/ml Taq polymerase, 100µM of the forward (PCO_3), and reverse primers (CD6, T_m = 58 ℃) dNTP mix (10mM each), DNA template, and H_2O. Initial denaturation was carried out at 94 ℃ for 2 minutes, followed by 35 cycles of repetitive denaturation at 94 ℃ for 30 seconds, annealing at 57 ℃ for 30 seconds, and extension at 68 ℃ for 1 minute. The samples were held at 4 ℃ prior to the agarose gel electrophoresis protocol.

For 10µL of the PCR samples, 10 µL of Orange G loading dye and 5 µL of 100 bp DNA ladder were added and then loaded into 1 % agarose gel with ethidium bromide. The gel was run at 150 volts (150 V) for 1 hour. The gel was then visualized with Gel Documentation & Analysis System (Beijing Liuyi Instrument Factory).

Citation: Abourajab A, Mostafanejad SM, Dinleyici M, Al-Khateeb B, Kunter I, et al. (2023) Synthesis, characterization, anti-cancer evaluation, and DNA-binding study of new bay-substituted perylene derivatives. J Biol Med 7(1): 031-043. DOI: https://dx.doi.org/10.17352/jbm.000039

G-quadruplex formation assay

The DNA binding capability of compounds **4** and **6** was detected by agarose gel electrophoresis assay. The compound/DNA complexes were loaded on a 4 % agarose gel. The gel was loaded with 5 µL of 100 bp DNA ladder, 10 µL of PCR product, and 10 µL of the perylene derivative (starting with a 2.5 µM concentration and increasing that by two-fold each time).

Cell culture and cytotoxicity assay

HCC cell line SK-HEP-1 was kindly provided by Prof. Dr. Esra Erdal (Izmir Biomedicine and Genome Centre, Izmir, Turkey). The cells were maintained in DMEM (cultured cell lines in Dulbecco`s modified eagle medium) supplemented with 10 % FBS (heat-inactivated fetal bovine serum), 100 µ/ml penicillin, 2mM L-glutamine, 100 mg/ml streptomycin and 1X NEAA at 5 % CO_2 at 37 ℃. MTT assay was used to determine the cytotoxic and anti-cancer effects of compounds **4** and **6** on SK-HEP-1 cancer cell lines for 48 hours. Cells were seeded onto 48-well plates at a density of 5 x 10^3 cells/ml and treated with different concentrations of the compounds. DMSO was used as a negative solvent control. Even though the final concentration of DMSO was less than 1% in all treatments, the effect of DMSO was evaluated on the SK-HEP-1 cell line. The effect of DMSO at max compound concentrations was found to be nonsignificant. Following the 48-hour treatment, 0.5 mg/ml MTT [3-(4,5-dimethylthiazol2-yl)-2,5-diphenyltetrazolium bromide] was added to the medium and incubated for 4 h at 37 ℃ in dark. The formazan crystals were dissolved with DMSO. The absorbance was measured at 570 nm using a microplate reader. The percentage of cell viability was calculated from the percent ratio of the absorbance obtained from each treatment and control. Experiments have been carried out three times independently.

Statistical analysis

All samples were presented as mean ± SE from 4 measurements for cytotoxicity analysis. A one-way ANOVA test with Tukey's correction for multiple comparisons was used for MTT analysis. A $p < 0.05$ was considered statistically significant. (* $p < 0.05$ *** $p < 0.001$). Data points were compared with the control. All the analyses were performed using GraphPad Prism 5 software.

Results and discussion

Synthesis and characterization of compounds 4 and 6

A two-step synthetic route toward the targeted compounds **4** and **6** is displayed in Scheme 1. In the first step, compound Br-PDA was prepared via catalytic bromination of perylene-3,4,9,10-tetracarboxylic anhydride (PDA) according to our previously reported procedures [33-37]. This step was followed by the synthesis of 1,7-di(3,5-diamino-pyrimidoxyl) perylene-3,4,9,10- tetracarboxylic acid bisanhydride (**4**) and 1,7-di(2-[3-[(4-amino-2-methylpyrimidin-5-yl)methyl]-4-methyl-1,3-thiazol-3-ium-5-yl]) ethoxyperylene-3,4,9,10-tetracarboxylic bisanhydride (**6**) via nucleophilic aromatic substitution reactions on 1,7-dibromoperylene-3,4,9,10-tetracarboxylic acid bisanhydride. Both compounds were characterized by NMR, Mass, IR, UV–vis, DSC, TGA, and elemental analysis. All data were consistent with the assigned structures, as shown in Scheme 1. The compounds exhibited good solubility in amide-type polar aprotic solvents like N-methyl-2-pyrrolidone (NMP), dimethyl sulfoxide (DMSO), and N, N-dimethylacetamide (DMAc), and even in less polar solvents like pyridine and trifluoroacetic acid (Table **2**). Notably, the colour of compounds **4** and **6** solutions in NMP, DMAc, DMF, and DMSO was the same as dark brown, possibly due to similar intra- and intermolecular H bonding interactions (N - H....O and N - H....N). The three-dimensional (3D) molecular structures of compounds **4** and **6** at different energy levels (all generated using MarvinSketch by ChemAxon) clearly show the different intra- and intermolecular interaction possibilities (Scheme 2). MarvinSketch for energy minimization provided the best results for the most stable conformation of the structures for compounds **4** and **6** with the lowest energy, as shown in Scheme 2 (lowest energy for compound **4**: 136.82 (a) and **6**: 212.01 kcal/mol (b)).

All FT-IR spectra were consistent with the assigned structures, as shown in Figure 1. The FT-IR spectrum of compound **4** exhibited characteristic absorption bands at 2000-3550 (centred near 3385, H-bonded broad stretching vibrational band of N-H stretch), 3015 (aromatic C-H stretch), 1756 and 1706 (hydrogen bonding broad anhydride C = O stretch), 1630 (C = N stretch), 1587 (aromatic C = C stretch), 1392 (amine C - N stretch), 1249 (ether C - O - C stretch), 1010 (anhydride C - O - C stretch), 766 cm^{-1} (aromatic C - H bend). For compound **6** characteristic absorption bands were also observed at 2000 - 3550 (centred near 3416, H-bonded broad stretching vibrational band of N - H stretch), 2921 and 2852 (aliphatic C-H stretch), 1756 and 1731 (hydrogen bonding broad anhydride C = O stretch), 1630 (C = N stretch), 1587 (aromatic C = C stretch), 1406 (amine C - N stretch), 1230 (ether C—O - C stretch), 1017 (anhydride C - O - C stretch), 735 cm^{-1} (aromatic C - H bend) (Figure 1). Notably, the hydrogen-bonding interaction through the bay positions hindered the π-π interactions of the molecules.

The ^{1}H NMR spectra were recorded with a 400 MHz pulsed Fourier transform NMR spectrometer in the solvent mixture $CDCl_3$:CF_3COOD (3:1) at room temperature. The chemical shifts are quoted relative to $CDCl_3$ and CF_3COOD [δ ($CDCl_3$) = 7.19 ppm; δ (CF_3COOD) = 11.61 ppm]. Importantly, the aromatic C-H signals of compound **6** in its ^{1}H NMR spectra were observed mainly, confirming the purity of the compound (Figure S2). The ^{1}H NMR of CF_3COOD confirmed that the impurity peaks shown in the aliphatic range belonged to CF_3COOD (Figure S3). Expectedly, the ^{1}H NMR spectra recorded in the solvent mixture $CDCl_3$: CF_3COOD (3:1) at room temperature for both products showed a significant signal broadening in the aromatic region caused by hydrogen bond-directed aggregation. Most probably, the different conformations are affecting its aggregation and intermolecular interactions.

On the other hand, all our attempts for NMR measurements of compound **4** were not successful due to poor solubility. Finally, despite all dilution conditions applied in different

Citation: Abourajab A, Mostafanejad SM, Dinleyici M, Al-Khateeb B, Kunter I, et al. (2023) Synthesis, characterization, anti-cancer evaluation, and DNA-binding study of new bay-substituted perylene derivatives. J Biol Med 7(1): 031-043. DOI: https://dx.doi.org/10.17352/jbm.000039

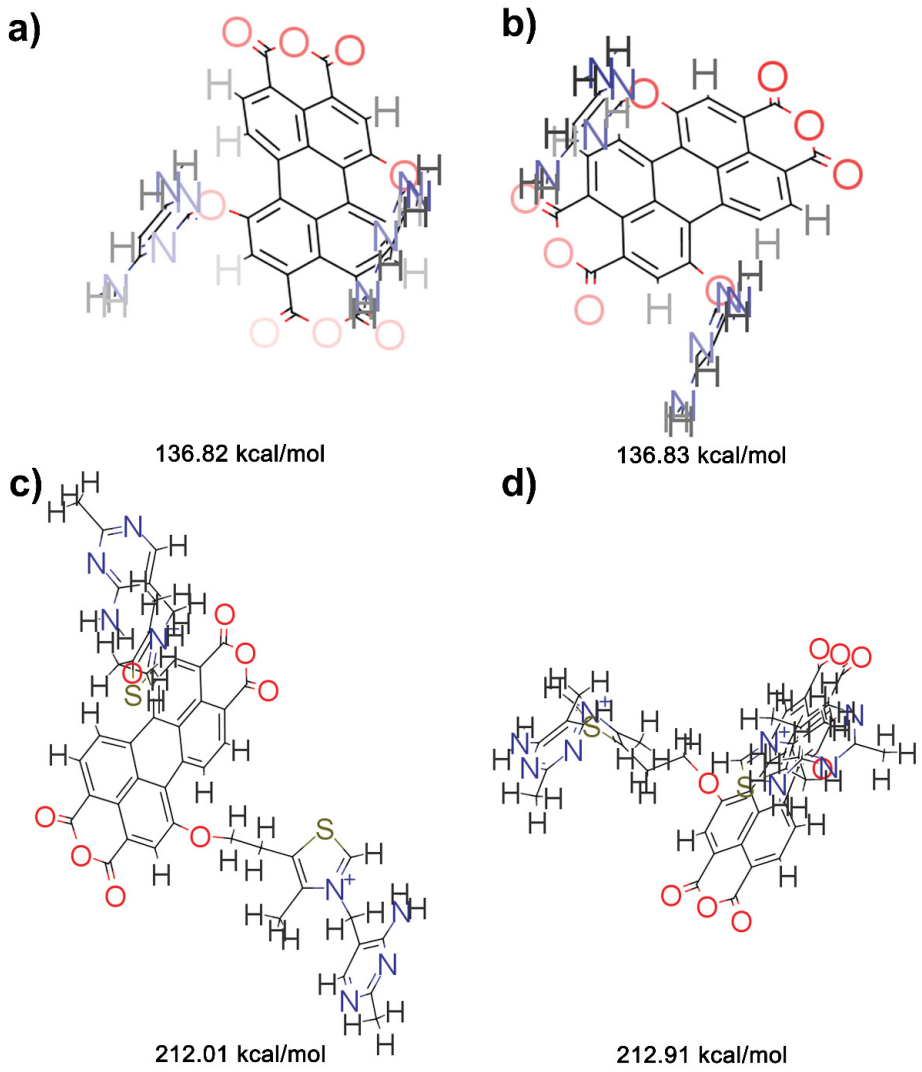

Scheme 2: Representative 3D molecular structures of compound **4** and Representative 3D molecular structures of compound **6** at different energy levels (all rendered using Marvin by Chem Axon).

Table 2: Maximum absorption wavelength λ_{max} (nm), molar extinction coefficient ε_{max} (mol^{-1} dm^3 cm^{-1}), oscillator strength ƒ, fluorescence quantum yield Φ_f (λ_{exc} = 485 nm), radiative life time τ_0 (ns), fluorescence life time τ_f (ns), fluorescence rate constant k_f (10^8 s^{-1}), rate constant of radiationless deactivation k_d (10^8 s^{-1}), and singlet energy E_s (kcal mol^{-1}) data of **4** and **6**.

Compound	Solvent	λ_{max}	ε_{max}	ƒ	Φ_f	τ_0	τ_f	k_f	k_d	E_s
4	NMP	518	12000	0.119	0.01	34.09	0.34	0.29	29.0	55.2
	DMAc	518	7800	0.073	0.02	55.97	1.12	0.18	8.76	55.2
	DMF	518	9500	0.104	0.30	39.01	11.70	0.26	0.60	55.2
6	NMP	518	33000	0.246	0.11	16.50	1.82	0.61	4.90	55.2
	DMAc	518	27000	0.237	0.10	17.14	1.71	0.58	5.25	55.2
	DMF	518	37000	0.223	0.23	18.22	4.19	0.55	1.84	55.2

solvents, the ^{13}C NMR spectroscopic measurements failed for both compounds. This property was attributed to the residual aggregation of the compounds in the selected deuterated solvents.

UV-vis absorption and fluorescence spectroscopy measurements

The interaction of compounds **4** and **6** with the oligonucleotides a-coreTT and c-kit was studied using UV-visible and fluorescence spectroscopies (Figures 3-5, S4). A fixed concentration of oligonucleotides (10 M) was titrated with increasing concentrations of compounds **4** and **6** (2.5 µM, 5 µM, 10 µM, and 20 µM). Spectra were scanned from 200 to 800 nm, and baseline correction was done using 1 M Tris-HCl (pH 7.4). Absorption and fluorescence measurements of the oligonucleotides and compound complexes were done with a concentration ratio of 1:2 and after 3 hours of incubation at room temperature and darkness without any disturbance (emission spectra: compounds **4** and **6**, λ_{exc} = 485 nm; complexes, λ_{exc} = 485 nm; pure primers, λ_{exc} = 250 nm).

Citation: Abourajab A, Mostafanejad SM, Dinleyici M, Al-Khateeb B, Kunter I, et al. (2023) Synthesis, characterization, anti-cancer evaluation, and DNA-binding study of new bay-substituted perylene derivatives. J Biol Med 7(1): 031-043. DOI: https://dx.doi.org/10.17352/jbm.000039

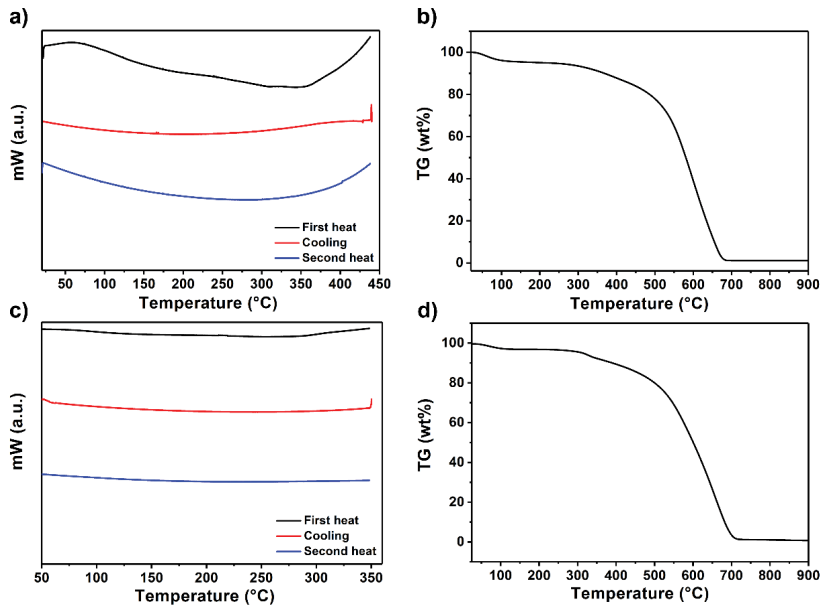

Figure 3: (a and c) DSC thermograms for 4 and 6 and (b and d) TGA curves for **4** and **6** at a heating rate of 10 ℃ per minute.

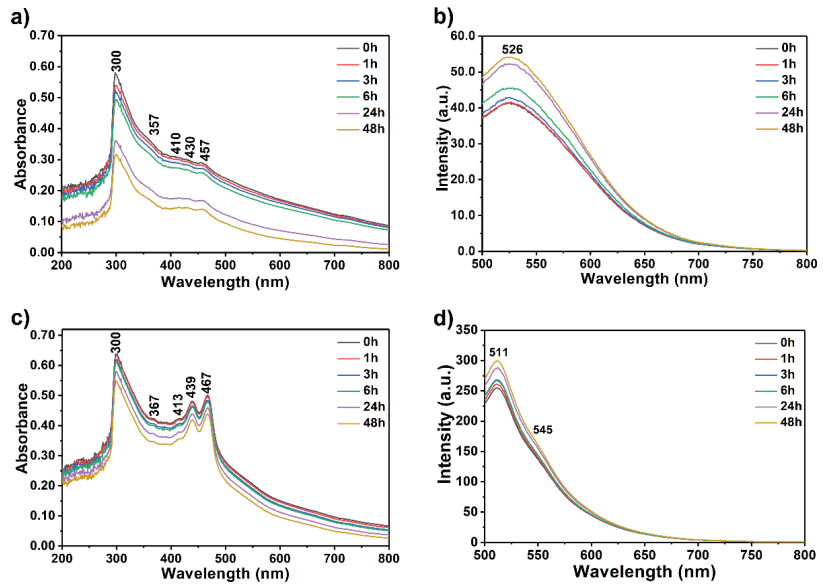

Figure 4: Absorbance (a and c) and Fluorescence (b and d) Spectra (λ_{exc} = 485 nm) of **4** and **6** at 20 µM.

First, 20 µM of each compound in Tris-HCl buffer solution (pH 7.4) was separately used to investigate their aggregation behaviour in regular time intervals from 0 to 24 h as a reference to track the interaction of the compounds with the oligonucleotides (Figure 4). The compound solutions were prepared using a sonicator and kept undisturbed at room temperature in darkness 1, 3, 6, 24 and 48 h before measuring absorbance and fluorescence. Afterward, the absorbance and emission spectra of the oligonucleotides alone were recorded to compare with the complexation results between the compounds and oligonucleotides (a-coreTT and c-kit; λ_{exc} = 220 nm, 10 µM, Figure 4). Then, recorded the absorbance and emission spectra of the compounds both in the absence and presence of the oligonucleotides in Tris-HCl buffer solution was recorded (Figure 5 and S4 pH 7.4).

Optical properties of compounds 4 and 6

Figure 2 shows the absorption and emission spectra of **4** and **6** in dipolar aprotic solvents such as PYR, NMP, DMAc, DMF, and DMSO and polar protic solvent TFAc at room temperature (1.0×10^{-5} M, Table 1). The UV–vis absorption bands of compounds **4** and **6** cover a large part of the visible spectrum (Figure 2a and **c**; 250 – 800 nm). As can be seen from both compounds' UV spectra, the sharp absorption peak around 300 nm is due to the bay substituents and the peaks in the range of 400–800 nm belong to perylene derivatives. Accordingly, compound **4** showed one sharp absorption peak around 306 nm following broad peaks in all studied solvents (Figure 2a, DMF: 468, 518 nm). The intramolecular hydrogen

Citation: Abourajab A, Mostafanejad SM, Dinleyici M, Al-Khateeb B, Kunter I, et al. (2023) Synthesis, characterization, anti-cancer evaluation, and DNA-binding study of new bay-substituted perylene derivatives. J Biol Med 7(1): 031-043. DOI: https://dx.doi.org/10.17352/jbm.000039

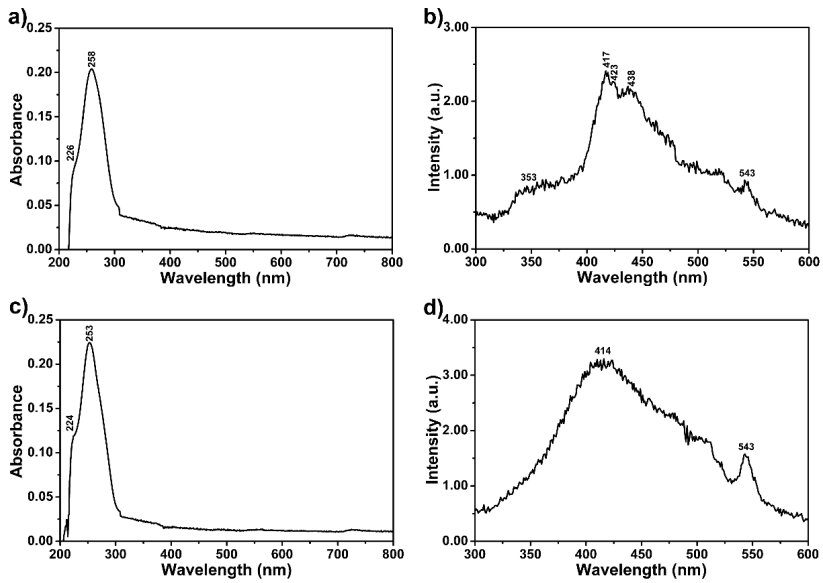

Figure 5: Absorbance (a and c) and Fluorescence (b and d) Spectra (λ_{exc} = 220 nm) of a-coreTT and c-kit at 10 µM.

bonding interactions probably caused this broadness (Schemes S1 and S2).

Notably, hydrogen bond-directed aggregation affected both compounds' absorption wavelengths. Similarly, compound **6** showed a similar sharp absorption peak around 302 nm and three broad peaks due to intermolecular hydrogen bonding interactions (Figure 2b, DMF: 417, 487, 518 nm). On the other hand, the broad long-wavelength absorption bands in dipolar aprotic solvents such as PYR, NMP, DMAc, DMF, and DMSO indicate the solvent-dependent aggregation behaviour of both compounds (Figure 2; compound **4**: 664 and compound **6**: 686 nm in NMP). This is confirmed, taking the molar absorption coefficient values into account (Table 1, molar absorption coefficients at 0-0 bands for **4**: 9500; and **6**: 37000 $mol^{-1}dm^3cm^{-1}$ in DMF). The absorption spectra of compounds **4** and **6** in Figures 2a and **c** are characteristic of a J-type aggregate (head-to-tail interactions) with a structured band centred around 700 nm, in agreement with our previous reports [33,35]. The results establish that hydrogen bonding (N–H...N) between substituents of the compounds effectively affects aggregation formation in those solutions. The shape of the aggregation band remained the same upon filtration of the compound solutions through a 0.2 m SPR microfilter. Notably, the size of the aggregates is less than 0.2 µm. On the other hand, in the absorption spectra taken in TFAc, the bands around 700 nm disappeared, probably due to the Haggregation (Figure 2).

The fluorescence spectra of compounds **4** and **6** were taken at λ_{exc} = 485 nm, and the relative fluorescence quantum yields were determined in NMP, DMAc, and DMF using N,N′-bis-dodecyl-3,4,9,10-perylenebis(dicarboximide) in CHL as standard (N,N′-bis-dodecyl-3,4,9,10-perylenebis(dicarboximide); Φ_f = 1 with respect to rhodamine 101 in ethanol) (Table 1, Figures 2a,d) [38-44]. The lower fluorescence quantum yields of both compounds could be attributed to conformational changes, torsional movement, or other non-radiative decays (compound **4**; NMP: 10 %, DMAc: 20 %, and DMF: 30 % and compound **6**; NMP: 11 %, DMAc: 10 % and DMF: 23 %). This dramatic fluorescence quenching results were attributed to photoinduced intramolecular electron transfer from the electron-donating substituents to the electron-accepting perylene core (Figure S5).

The emission spectra of compound **4** taken in all studied solvents showed red-shifted and broad excimer-like emissions attributed to the formation of ground-state hydrogen complexes with limited π–stacking interaction in solutions (Figure 2b and d; λ_{exc} = 485 nm). Interestingly, a new red-shifted emission band appeared at 719 nm in the solvents DMSO and NMP, attributed to the formation of J-aggregates promoted by hydrogen bonding between molecules. The peak at 719 nm disappeared in the other solvents, probably due to the H-aggregates. On the other side, fluorescence spectra of compound **6** showed blue shifted and well-separated three bands without any excimer formation. This property is attributed to weakening intermolecular hydrogen bonds in the electronically excited state.

Optical parameters such as maximum absorption wavelength (λ_{max}, nm), molar absorption coefficient (ε_{max}, $mol^{-1}dm^3cm^{-1}$), oscillator strength (f), fluorescence quantum yield (Φ_f), theoretical radiative lifetime (τ_0, ns), fluorescence lifetime (τ_f, ns), fluorescence rate constant (k_f, s^{-1}), the rate constant of radiationless deactivation (k_d, s^{-1}) and singlet energy (E_s, kcal mol^{-1}) data of compounds **4** and **6** in NMP, DMAc and DMF are given in Table **1**, respectively. The theoretical radiative lifetimes (τ_0) were calculated according to the formula: $\tau_0 = 3.5 \times 10^8/(\nu^2_{max}\, \varepsilon_{max}\, \Delta\nu_{1/2})$, where ν_{max} stands for the wavenumber in cm^{-1}, ε_{max} for the molar absorption coefficient at the selected absorption wavelength and $\Delta\nu 1/2$ indicates the half-width of the desired absorption in units of cm-1 [43,44].

Citation: Abourajab A, Mostafanejad SM, Dinleyici M, Al-Khateeb B, Kunter I, et al. (2023) Synthesis, characterization, anti-cancer evaluation, and DNA-binding study of new bay-substituted perylene derivatives. J Biol Med 7(1): 031-043. DOI: https://dx.doi.org/10.17352/jbm.000039

Thermal stability

The thermal properties of compounds **4** and **6** were investigated by differential scanning calorimetry (DSC) and thermogravimetric analysis (TGA), as shown in Figure **6** (heating rate: 10 ℃ min^{-1}, DSC: nitrogen atmosphere, temperature range of 30 ℃ - 900 ℃ and TGA: oxygen atmosphere, 30 ℃ - 900 ℃). Compounds **4** and **6** exhibit no glass transition temperature during the first and second heating DSC runs, as shown in Figure 6a and c. The DSC curves revealed that the decomposition temperatures (T_d) were above 375 °C, which is also evident from the TGA curves in Figure 6b and d. Remarkably, both compounds showed high thermal stability, which could be attributed to perylene's rigid chromophoric structure (decomposition starting temperature; compound **4**: 500 and compound **6**: 478 ℃). Upon heating to 700 °C, both compounds lost 98 % of their initial weight, and a 2 % char yield was obtained.

Interaction of compounds 4 and 6 with oligonucleotides

UV–visible and fluorescence spectroscopic studies: Absorption spectroscopy is a versatile way to determine the binding strength and the mode of DNA with small molecules. In the present study, compounds **4** and **6** were investigated for their interactions with oligonucleotides via UV–vis absorption spectroscopy (Table 3, Figures 3-5 and S4; oligonucleotides: a-coreTT and c-kit). The UV-vis spectra with increasing concentrations of compounds **4** and **6** were recorded in the absence and presence of oligonucleotides.

At first, the UV-vis absorption and emission spectra of compounds in the absence of oligonucleotides in Tris-HCl buffer solution were recorded at regular time intervals to observe their aggregation behaviour (Figure 3, λ_{exc} = 485 nm, 20 µM; from 0 to 48 h). The compound solutions were prepared using a sonicator and kept undisturbed at room temperature in darkness for 1, 3, 6, 24, and 48 h before measuring absorbance and fluorescence. Compound **4** showed a higher aggregation tendency than compound **6** after 24 hours, as shown in Figures 3a and c. On the other hand, the emission for both compounds was intensified upon increasing the time interval attributed to the possible intramolecular energy transfer process within the molecules (Figure 3).

The interaction of compounds **4** and **6** with the oligonucleotides a-coreTT and c-kit was studied using UV-vis and fluorescence spectroscopies (Figures 5 and S4). A fixed concentration of oligonucleotides (10 µM) was titrated with increasing concentrations of compounds **4** and **6** (2.5 µM, 5 µM, 10 µM, and 20 µM). The spectra were scanned from 200 to 800 nm, and baseline correction was done using 1M Tris-HCl (pH 7.4). The addition of the a-coreTT to a solution of compound **4** induces remarkable shifts in λ_{max} and absorption intensity (Figure 5). Upon increasing the concentration of the compound, the absorption band belonging to the bay substituent at 300 nm showed gradual hyperchromic and hypsochromic shifts and finally reached a maximum of 20 µM (Figures 5). The band shifted to 216 nm and intensified eight times more than pure a-coreTT. Importantly, similar behaviour was observed for the oligonucleotide c-kit (Figures 5 and S4). The increase in the absorption (hyperchromic) of compound **4** in the presence of a-coreTT and c-kit suggests a non–intercalation mode of interaction through electrostatic forces, van der Waals interactions, dative bonds, hydrogen bonds, and hydrophobic interactions (Figures 5 and S4). The hyperchromic effect is due to the electrostatic binding of compound **4** with

Table 3: List of the Oligonucleotides with their Sequences.

Name of Oligonucleotide	Sequence (5′-3′)
PCO3(F)	ACACAACTGTGTTCACTAGC
CD6(R)	ATTCGTCTGTTTCCCATTCTAAAC
a-coreTT	AGGGTTAGGGTTAGGGTTAGGGTT
c-kit	AGGGAGGGCGCTGGGAGGAGGAGGG

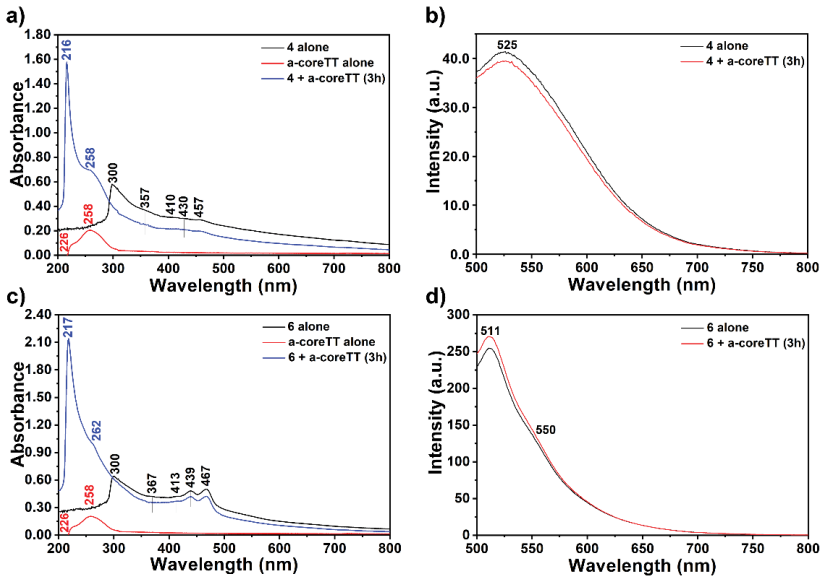

Figure 6: Absorbance (a and c) and Fluorescence (b and d) Spectra (λ_{exc} = 485 nm) of **4** and **6** with a-coreTT with a 2:1 concentration ratio.

Citation: Abourajab A, Mostafanejad SM, Dinleyici M, Al-Khateeb B, Kunter I, et al. (2023) Synthesis, characterization, anti-cancer evaluation, and DNA-binding study of new bay-substituted perylene derivatives. J Biol Med 7(1): 031-043. DOI: https://dx.doi.org/10.17352/jbm.000039

the a-coreTT involving the hydrogen-bonding interaction between coordinated -C = O with functional groups positioned on the edge of oligonucleotide bases. Therefore, the maximum exposure of base pairs to the light increases the absorption intensity; hence, a hyperchromic shift occurs (Figure 5a).

Similarly, when the a-coreTT was added to compound **6** solutions, upon increasing the concentration of the compound, the absorption band belonging to the bay substituent at 300 nm showed gradual hyperchromic and hypsochromic shifts. Finally, it reached a maximum of 20 µM (Figures 5 and S4). Interestingly, the band shifted to 217 nm and intensified fourteen times more than pure a-coreTT. Furthermore, a-coreTT's absorption band at 258 nm intensified and shifted to 262 nm.

In general, non-intercalative binding includes groove binding and electrostatic interactions. Groove binding involves hydrogen bonds and van der Waals forces and allows compounds to bind through the grooves of the oligonucleotide (supporting H-bonding). The electrostatic interaction occurs between compound **4** and oligonucleotides a-coreTT or c-kit through the high negative charge on the oligonucleotide's phosphate backbone. It is important to note that the electrostatic interaction occurs between compound **6** and oligonucleotides a-coreTT or c-kit through the high negative charge on the oligonucleotide's phosphate backbone and the positive charge on the interacting molecule. Hence, compound **6** performed much better binding to the a-coreTT or c-kit than **4**. The absorption spectra of the complexes of the compounds with a-coreTT and c-kit (Figures 4,5 and S4) show no alteration in the perylene core's absorption peaks.

The fluorescence spectra (Figures 5 and S4) of compounds-oligonucleotide complexes showed broad excimer-like emissions (λ_{exc} = 485 nm) like the emissions observed for compounds **4** and **6** (Figure 2). There was little change in the emission spectra for compounds-oligonucleotide complexes. Notably, the compounds bind to oligonucleotides via non-intercalative binding mode.

G-quadruplex formation assay: G-quadruplex structures (G4) are biologically important conformations formed by folding Guanine-rich nucleic sequences into four-stranded DNA secondary structures. The presence of G4 structures within oncogenic promoters and at telomeres causes them to downregulate transcription or block telomere elongation in cancer cells. Notably, effective G4 stabilizing compounds are promising alternatives in cancer therapeutics.

In detail, compounds **4** and **6** interaction as G4 stabilizers with G4 former human beta-globin gene were investigated using the 595 bp PCR amplified region and agarose gel electrophoresis (4 %). Polymerase Chain Reaction (PCR) [44] was carried out for a guanine-rich region of the beta-globin gene (exon I, exon II, and 60bp of intron II after exon II) from the isolated human DNA. PCR amplification was performed with 1X PCR buffer, 5 u/ml Taq polymerase, 100 µM of the forward (PCO_3), and reverse (CD6) primers (Tm = 58 °C) dNTP mix (10mM each), DNA template, and H_2O.

Agarose gel electrophoresis resolves DNA fragments based on their molecular weight. Therefore, the bands with the PCR product alone are expected to migrate longer distances on the gel than the bands that contain the PCR product and the perylene derivative complex. The band migrations were compared with each other with the help of a straight line illustrating equal distance migrated from the wells up until the straight line originating from the DNA ladder (Figure **7**). The difference in path length observed with the help of the straight line could be attributed to the formation of a G4 structure (Lane A: DNA ladder; Lane B: PCR product alone; Lanes F-H: PCR product and compound **4** in 2.5, 5 and 10 µM concentrations; Lanes I-K: PCR product and compound **6** in 2.5, 5 and 10 µM concentrations). Notably, compound **6**'s migration was slower compared to compound **4**.

It is important to note here that compound **6** has a positive charge on its structure besides the hydrogen bonding potential of compounds **4** and **6**, enhancing its potential to interact strongly with the negatively charged oligonucleotide backbone [4]. The other possible reason for the slower migration of compound **6** could be its higher molecular mass (compound **4**: 640.52 g/mol compound **6**: 918.99 g/mol).

Notably, a concentration-dependent migration for the bands containing the PCR product and compound **4** was observed (Figure **7**, Lanes F-H). More importantly, the migration bands for compound **6** were much more slowly than those belonging to compound **4** (Figure **7**, Lanes I-K: migration of the band at 2.5 µM concentration for compound **4** is equal to the band's migration at 10 µM concentration of compound **4**). Most probably, the positive charge on the substituents of compound **6** strengthens its G4 stabilizing potency.

MTT assay on SK-HEP-1 adenocarcinoma cells: In the present study, the effect of the compounds investigated on the SK-HEP-1 cell line which is widely used for liver carcinoma research and closely mimics liver cancers. Evaluation of the anti-cancer activity of compounds **4** and **6** was investigated using the MTT assay on the SK-HEP-1 cell line (Figure 8). Notably, the level of cytotoxicity potency of the compounds is concentration dependent. As depicted in Figure 8, each of the applied concentrations of these compounds has a different

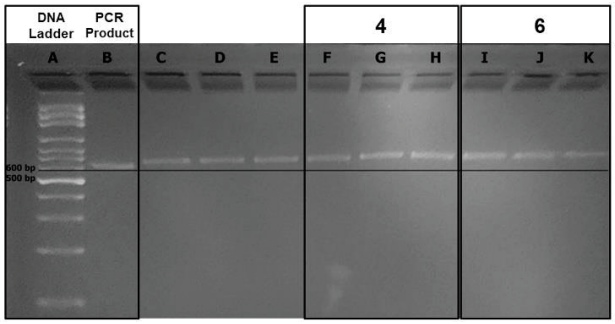

Figure 7: Results of G-Quadruplex Formation Assay on 4% Agarose Gel. Lane A illustrates the DNA ladder, lane B illustrates the PCR product alone, lanes C through E illustrate the complex of PCR product and two-fold concentrations (2.5µM – 10µM) of **4**, lanes F through H illustrate the complex of PCR product and two-fold concentrations (2.5µM – 10µM) of **6**.

Citation: Abourajab A, Mostafanejad SM, Dinleyici M, Al-Khateeb B, Kunter I, et al. (2023) Synthesis, characterization, anti-cancer evaluation, and DNA-binding study of new bay-substituted perylene derivatives. J Biol Med 7(1): 031-043. DOI: https://dx.doi.org/10.17352/jbm.000039

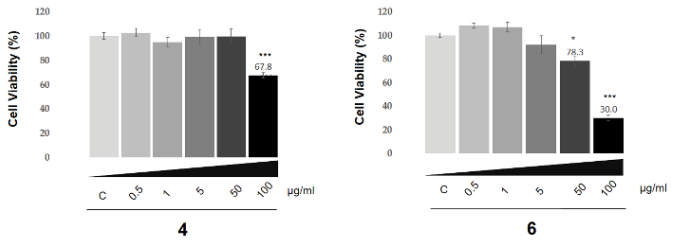

Figure 8: Anti-cancer Effects of **4** and **6** on SK-HEP-1 Cancer Cell Lines.

level of cytotoxicity potency. The viability of the SK-HEP-1 adenocarcinoma cell line has significantly decreased above 100 µg/ml and 50 µg/ml for compounds **4** and **6**, respectively. The IC_{50} values were calculated as 79.6 µg/ml for compound **4** and 50.9 µg/ml for compound **6**. Compound **6** showed moderate anticancer activity. The effectivity level of compound **6** is higher than compound **4** in terms of anti-cancer activity according to the MTT assay and statistical analysis.

Conclusion

In summary, two bay-substituted perylene bisanhydrides were successfully designed and synthesized, and characterized through conventional spectroscopic methods. The interaction of those compounds with oligonucleotides, human beta-globin gene, and SK-HEP-1 adenocarcinoma cells was investigated using biophysical techniques. UV-vis and fluorescence spectroscopies were employed to study the interaction of the compounds with oligonucleotides. Our results demonstrated that compounds **4** and **6** are promising DNA-binding and cytotoxic compounds with a relatively antiproliferative effect on selected tumour cells, SK-HEP-1 adenocarcinoma, and even with a significant concentration-dependent selectivity. Within compounds **4** and **6**, the formal positive charge consisting of compound **6** showed the most pronounced effect. A guanine-rich region was successfully amplified from the human beta-globin gene via PCR. The complexation of this region with compounds **4** and **6** was investigated via agarose gel electrophoresis. It is noteworthy that compound **6** exhibited a more potent binding potential. Moreover, the MTT assay has shown that both dyes have decreased the SK-HEP-1 adenocarcinoma cell line viability at 100 µg/ml, with compound **6** indicating the highest potential. Furthermore, the absorption and fluorescence studies confirmed the non-intercalative interaction between the compounds and two different oligonucleotides. Absorption and fluorescence investigations showed probable energy transfer from the primers and substituents on the compounds to the perylene aromatic core. Finally, based on this study's encouraging results, it could be concluded that these properties warrant further studies of this class of compounds as a new promising structure for antitumor agents. Future studies aim to focus on detailed investigations to synthesize and identify even more potent perylene derivatives with efficient and selective antitumor activity in different cell lines.

Acknowledgement

The support from Eastern Mediterranean University BAP-Projects Research Funding (BAPC-04-21-03) is acknowledged.

Supporting information summary

Supplementary material is available on the publisher's website along with the published article.

(**Supplementary Material**)

References

1. Taka T, Joonlasak K, Huang L, Randall Lee T, Chang SW, Tuntiwechapikul W. Down-regulation of the human VEGF gene expression by perylene monoimide derivatives. Bioorg Med Chem Lett. 2012 Jan 1;22(1):518-22. doi: 10.1016/j.bmcl.2011.10.089. Epub 2011 Nov 6. PMID: 22104143.

2. Kaewtunjai N, Summart R, Wongnoppavich A, Lojanapiwat B, Lee TR, Tuntiwechapikul W. Telomerase Inhibition, Telomere Shortening, and Cellular Uptake of the Perylene Derivatives PM2 and PIPER in Prostate Cancer Cells. Biol Pharm Bull. 2019 Jun 1;42(6):906-914. doi: 10.1248/bpb.b18-00860. Epub 2019 Mar 30. PMID: 30930403.

3. D'Ambrosio D, Reichenbach P, Micheli E, Alvino A, Franceschin M, Savino M, Lingner J. Specific binding of telomeric G-quadruplexes by hydrosoluble perylene derivatives inhibits repeat addition processivity of human telomerase. Biochimie. 2012 Mar;94(3):854-63. doi: 10.1016/j.biochi.2011.12.004. Epub 2011 Dec 9. PMID: 22182489.

4. Summart R, Thaichana P, Supan J, Meepowpan P, Lee TR, Tuntiwechapikul W. Superiority of an Asymmetric Perylene Diimide in Terms of Hydrosolubility, G-Quadruplex Binding, Cellular Uptake, and Telomerase Inhibition in Prostate Cancer Cells. ACS Omega. 2020 Nov 12;5(46):29733-29745. doi: 10.1021/acsomega.0c03505. PMID: 33251409; PMCID: PMC7689663.

5. Chen H, Guan Y, Yuan G, Zhang Q, Jing N. A perylene derivative regulates HIF-1α and Stat3 signaling pathways. Bioorg Med Chem. 2014 Feb 15;22(4):1496-505. doi: 10.1016/j.bmc.2013.10.018. Epub 2013 Oct 24. PMID: 24485121.

6. GELLERT M, LIPSETT MN, DAVIES DR. Helix formation by guanylic acid. Proc Natl Acad Sci U S A. 1962 Dec 15;48(12):2013-8. doi: 10.1073/pnas.48.12.2013. PMID: 13947099; PMCID: PMC221115.

7. Hänsel-Hertsch R, Spiegel J, Marsico G, Tannahill D, Balasubramanian S. Genome-wide mapping of endogenous G-quadruplex DNA structures by chromatin immunoprecipitation and high-throughput sequencing. Nat Protoc. 2018 Mar;13(3):551-564. doi: 10.1038/nprot.2017.150. Epub 2018 Feb 22. PMID: 29470465.

8. Edwards DN, Machwe A, Wang Z, Orren DK. Intramolecular telomeric G-quadruplexes dramatically inhibit DNA synthesis by replicative and translesion polymerases, revealing their potential to lead to genetic change. PLoS One. 2014 Jan 14;9(1):e80664. doi: 10.1371/journal.pone.0080664. PMID: 24454683; PMCID: PMC3891601.

9. Samudrala R, Zhang X, Wadkins RM, Mattern DL. Synthesis of a non-cationic, water-soluble perylenetetracarboxylic diimide and its interactions with G-quadruplex-forming DNA. Bioorg Med Chem. 2007 Jan 1;15(1):186-93. doi: 10.1016/j.bmc.2006.09.075. Epub 2006 Oct 10. PMID: 17079147.

10. Bochman ML, Paeschke K, Zakian VA. DNA secondary structures: stability and function of G-quadruplex structures. Nat Rev Genet. 2012 Nov;13(11):770-80. doi: 10.1038/nrg3296. Epub 2012 Oct 3. PMID: 23032257; PMCID: PMC3725559.

11. Rhodes D, Lipps HJ. G-quadruplexes and their regulatory roles in biology. Nucleic Acids Res. 2015 Oct 15;43(18):8627-37. doi: 10.1093/nar/gkv862. Epub 2015 Sep 8. PMID: 26350216; PMCID: PMC4605312.

12. Vorlíčková M, Chládková J, Kejnovská I, Fialová M, Kypr J. Guanine tetraplex topology of human telomere DNA is governed by the number of (TTAGGG) repeats. Nucleic Acids Res. 2005 Oct 12;33(18):5851-60. doi: 10.1093/nar/gki898. PMID: 16221978; PMCID: PMC1253834.

Citation: Abourajab A, Mostafanejad SM, Dinleyici M, Al-Khateeb B, Kunter I, et al. (2023) Synthesis, characterization, anti-cancer evaluation, and DNA-binding study of new bay-substituted perylene derivatives. J Biol Med 7(1): 031-043. DOI: https://dx.doi.org/10.17352/jbm.000039

13. Chu B, Yuan G, Zhou J, Ou Y, Zhu P. A New Telomerase Inhibitor and Apoptosis-Inducing Agent in Leukemia: Perylene Derivative G-Quadruplex Ligand Tel03. Drug Dev. Res. 2008; 69:235-241.

14. Chambers VS, Marsico G, Boutell JM, Di Antonio M, Smith GP, Balasubramanian S. High-throughput sequencing of DNA G-quadruplex structures in the human genome. Nat Biotechnol. 2015 Aug;33(8):877-81. doi: 10.1038/nbt.3295. Epub 2015 Jul 20. PMID: 26192317.

15. Kaulage MH, Maji B, Pasadi S, Ali A, Bhattacharya S, Muniyappa K. Targeting G-quadruplex DNA structures in the telomere and oncogene promoter regions by benzimidazole-carbazole ligands. Eur J Med Chem. 2018 Mar 25;148:178-194. doi: 10.1016/j.ejmech.2018.01.091. Epub 2018 Feb 5. PMID: 29459277.

16. Rankin S, Reszka AP, Huppert J, Zloh M, Parkinson GN, Todd AK, Ladame S, Balasubramanian S, Neidle S. Putative DNA quadruplex formation within the human c-kit oncogene. J Am Chem Soc. 2005 Aug 3;127(30):10584-9. doi: 10.1021/ja050823u. PMID: 16045346; PMCID: PMC2195896.

17. Street STG, Chin DN, Hollingworth GJ, Berry M, Morales JC, Galan MC. Divalent Naphthalene Diimide Ligands Display High Selectivity for the Human Telomeric G-quadruplex in K^+ Buffer. Chemistry. 2017 May 23;23(29):6953-6958. doi: 10.1002/chem.201700140. Epub 2017 Mar 30. PMID: 28257554; PMCID: PMC5485019.

18. Zhang LN, Zhang R, Cui Y, et al. Highly specific G-quadruplex recognition covering physiological pH range by a new water-soluble cationic porphyrin with low self-aggregation tendency. Dyes and Pigm. 2017; 145:404-417.

19. Bejugam M, Sewitz S, Shirude PS, Rodriguez R, Shahid R, Balasubramanian S. Trisubstituted isoalloxazines as a new class of G-quadruplex binding ligands: small molecule regulation of c-kit oncogene expression. J Am Chem Soc. 2007 Oct 31;129(43):12926-7. doi: 10.1021/ja075881p. Epub 2007 Oct 5. PMID: 17918848; PMCID: PMC2195890.

20. Micheli E, Altieri A, Cianni L, Cingolani C, Iachettini S, Bianco A, Leonetti C, Cacchione S, Biroccio A, Franceschin M, Rizzo A. Perylene and coronene derivatives binding to G-rich promoter oncogene sequences efficiently reduce their expression in cancer cells. Biochimie. 2016 Jun;125:223-31. doi: 10.1016/j.biochi.2016.04.008. Epub 2016 Apr 13. PMID: 27086081.

21. Maleki P, Ma Y, Iida K, Nagasawa K, Balci H. A single molecule study of a fluorescently labeled telomestatin derivative and G-quadruplex interactions. Nucleic Acids Res. 2017 Jan 9;45(1):288-295. doi: 10.1093/nar/gkw1090. Epub 2016 Nov 29. PMID: 27899628; PMCID: PMC5224478.

22. Hu Y, Han D, Zhang Q, Wu T, Li F, Niu L. Perylene ligand wrapping G-quadruplex DNA for label-free fluorescence potassium recognition. Biosens Bioelectron. 2012 Oct-Dec;38(1):396-401. doi: 10.1016/j.bios.2012.06.042. Epub 2012 Jul 1. PMID: 22794931.

23. Rossetti L, Franceschin M, Schirripa S, Bianco A, Ortaggi G, Savino M. Selective interactions of perylene derivatives having different side chains with inter- and intramolecular G-quadruplex DNA structures. A correlation with telomerase inhibition. Bioorg Med Chem Lett. 2005 Jan 17;15(2):413-20. doi: 10.1016/j.bmcl.2004.10.061. PMID: 15603964.

24. Xu Z, Guo K, Yu J, Sun H, Tang J, Shen J, Müllen K, Yang W, Yin M. A unique perylene-based DNA intercalator: localization in cell nuclei and inhibition of cancer cells and tumors. Small. 2014 Oct 29;10(20):4087-92. doi: 10.1002/smll.201401262. Epub 2014 Jun 27. PMID: 24976526.

25. Sissi C, Lucatello L, Paul Krapcho A, Maloney DJ, Boxer MB, Camarasa MV, Pezzoni G, Menta E, Palumbo M. Tri-, tetra- and heptacyclic perylene analogues as new potential antineoplastic agents based on DNA telomerase inhibition. Bioorg Med Chem. 2007 Jan 1;15(1):555-62. doi: 10.1016/j.bmc.2006.09.029. Epub 2006 Oct 10. PMID: 17035038.

26. Rossetti L, Franceschin M, Bianco A, Ortaggi G, Savino M. Perylene diimides with different side chains are selective in inducing different G-quadruplex DNA structures and in inhibiting telomerase. Bioorg Med Chem Lett. 2002 Sep 16;12(18):2527-33. doi: 10.1016/s0960-894x(02)00504-8. PMID: 12182853.

27. Ceschi S, Largy E, Gabelica V, Sissi C. A two-quartet G-quadruplex topology of human KIT2 is conformationally selected by a perylene derivative. Biochimie. 2020 Dec;179:77-84. doi: 10.1016/j.biochi.2020.09.015. Epub 2020 Sep 16. PMID: 32949676.

28. Pasaogullari N, Icil H, Demuth M. Symmetrical and unsymmetrical perylene diimides: Their synthesis, photophysical and electrochemical properties. Dyes and Pigm. 2006; 69:118-127.

29. Vasimalla S, Sato S, Takenaka F, Kurose Y, Takenaka S. Cyclic perylene diimide: Selective ligand for tetraplex DNA binding over double stranded DNA. Bioorg Med Chem. 2017 Dec 15;25(24):6404-6411. doi: 10.1016/j.bmc.2017.10.014. Epub 2017 Oct 21. PMID: 29089258.

30. Avlasevich Y, Li C, Müllen K. Synthesis, and applications of core-enlarged perylene dyes. J. Mater. Chem. 2010;20:3814-3826.

31. Franceschin M, Nocioni D, Biroccio A, Micheli E, Cacchione S, Cingolani C, Venditti A, Zizza P, Bianco A, Altieri A. Design and synthesis of a new dimeric xanthone derivative: enhancement of G-quadruplex selectivity and telomere damage. Org Biomol Chem. 2014 Dec 21;12(47):9572-82. doi: 10.1039/c4ob01658k. Epub 2014 Nov 3. PMID: 25363232.

32. Xu Z, Cheng W, Guo K, Yu J, Shen J, Tang J, Yang W, Yin M. Molecular size, shape, and electric charges: essential for perylene bisimide-based DNA intercalator to localize in cell nuclei and inhibit cancer cell growth. ACS Appl Mater Interfaces. 2015 May 13;7(18):9784-91. doi: 10.1021/acsami.5b01665. Epub 2015 May 4. PMID: 25899704.

33. Dinleyici M, Al-Khateeb B, Abourajab A, et al. Synthesis, photophysical, electrochemical and DFT studies of two novel triazine-based perylene dye molecules. J. Photochem. Photobiol. A: Chemistry. 2021; 421:113525.

34. Mullis K, Faloona F, Scharf S, Saiki R, Horn G, Erlich H. Specific enzymatic amplification of DNA in vitro: the polymerase chain reaction. Cold Spring Harb Symp Quant Biol. 1986;51 Pt 1:263-73. doi: 10.1101/sqb.1986.051.01.032. PMID: 3472723.

35. Al-Khateeb B, Dinleyici M, Abourajab A, et al. Swallow tail bay-substituted novel perylene bisimides: synthesis, characterization, photophysical and electrochemical properties and DFT studies. J. Photochem. Photobiol A: Chemistry. 2020; 393:112432.

36. Mostafanejad SM, Bodapati JB, Özkar S, et al. Synthesis, characterization, photophysical and electrochemical properties of a new non-planar perylene diimide with electron donating substituent. Opt. Mater. 2018; 82:30-38.

37. Koyuncu S, Kus M, Demic S, et al. Electrochemical and Optical Properties of Novel Donor-Acceptor Thiophene-Perylene-Thiophene Polymers. J. Polym. Sci. 2008; 46:1974-1989.

38. Icli S, Icil H. Fluorescence Quantum Yields of Perylene 3,4,9,10-Tetracarboxylic Acid-bis-N, N'-aryl(alkyl) Diimides. Spectrosc. Lett. 1994; 27:323-332.

39. Icil H, Icli S. The Synthesis and Spectral Characteristics of a Supramolecular Model: Perylene 3,4,9,10-Tetracarboxylic Acid-bis-N, N'-p-aminophenyl Diimide. Spectrosc. Lett. 1995; 28:595-601.

40. Icil H, Uzun D, Arslan E. Synthesis and Spectroscopic Characterization of Water Soluble Perylene Tetracarboxylic Diimide Derivatives. Spectrosc. Lett. 2001; 34:605-614.

41. Ozser ME, Uzun D, Elci I, Icil H, Demuth M. Novel naphthalene diimides and a cyclophane thereof: synthesis, characterization, photophysical and electrochemical properties. Photochem Photobiol Sci. 2003 Mar;2(3):218-23. doi: 10.1039/b208856h. PMID: 12713220.

42. Uzun D, Ozser ME, Yuney K, et al. Synthesis and photophysical properties of N, N '-bis(4-cyanophenyl)-3,4,9,10-perylenebis(dicarboximide) and N, N '-bis(4-cyanophenyl)-1,4,5,8-naphthalenediimide. J. Photochem. Photobiol. A: Chemistry. 2003; 156:45-54.

Citation: Abourajab A, Mostafanejad SM, Dinleyici M, Al-Khateeb B, Kunter I, et al. (2023) Synthesis, characterization, anti-cancer evaluation, and DNA-binding study of new bay-substituted perylene derivatives. J Biol Med 7(1): 031-043. DOI: https://dx.doi.org/10.17352/jbm.000039

43. Bodapati JB, Icil H. A new tunable light-emitting and π-stacked hexa-ethyleneglycol naphthalene-bisimide oligomer: synthesis, photophysics and electrochemical properties. Photochem Photobiol Sci. 2011 Aug;10(8):1283-93. doi: 10.1039/c1pp05019b. Epub 2011 May 6. PMID: 21552597.

44. Bodapati JB, Icil H. A new tunable light-emitting and pi-stacked hexa-ethyleneglycol naphthalene-bisimide oligomer: synthesis, photophysics and electrochemical properties. J. Photochem. Photobiol. A: Chemistry.

Citation: Abourajab A, Mostafanejad SM, Dinleyici M, Al-Khateeb B, Kunter I, et al. (2023) Synthesis, characterization, anti-cancer evaluation, and DNA-binding study of new bay-substituted perylene derivatives. J Biol Med 7(1): 031-043. DOI: https://dx.doi.org/10.17352/jbm.000039